Phenomenology of diphoton photoproduction at next to leading order

Oskar Grocholski

Deutsches Elektronen-Synchrotron DESY

in collaboration with B. Pire, P. Sznajder, L. Szymanowski and J. Wagner.
[arXiv:2204.00396]

XXIX International Workshop
on Deep-Inelastic Scattering and Related Subjects

May 3, 2022

GPD extraction from exclusive experiments

GPD extraction from exclusive experiments

Consider a process on a nucleon N, in which a hard scale $|Q^2| \gg \Lambda_{QCD}$ is present.

GPD extraction from exclusive experiments

Consider a process on a nucleon N, in which a hard scale $|Q^2| \gg \Lambda_{QCD}$ is present.
Factorize the amplitude into perturbatively computable hard part and process-independent Generalised Parton Distributions.

GPD extraction from exclusive experiments

Consider a process on a nucleon N, in which a hard scale $|Q^2| \gg \Lambda_{QCD}$ is present.
Factorize the amplitude into perturbatively computable hard part and process-independent Generalised Parton Distributions.

- Deeply Virtual Compton Scattering: $e^- N \to e^- N \gamma$.
  The relevant hard sub-process: $\gamma^* N \to \gamma N$,

GPD extraction from exclusive experiments

Consider a process on a nucleon N, in which a hard scale $|Q^2| \gg \Lambda_{QCD}$ is present.
Factorize the amplitude into perturbatively computable hard part and process-independent Generalised Parton Distributions.

- Deeply Virtual Compton Scattering: $e^- N \to e^- N \gamma$.
  The relevant hard sub-process: $\gamma^* N \to \gamma N$,
- Timelike Compton Scattering: $\gamma N \to \gamma^* N$,

GPD extraction from exclusive experiments

Consider a process on a nucleon N, in which a hard scale $|Q^2| \gg \Lambda_{QCD}$ is present.
Factorize the amplitude into perturbatively computable hard part and process-independent Generalised Parton Distributions.

- Deeply Virtual Compton Scattering: $e^- N \to e^- N \gamma$.
  The relevant hard sub-process: $\gamma^* N \to \gamma N$,
- Timelike Compton Scattering: $\gamma N \to \gamma^* N$,
- Deeply Virtual Meson Production: $\gamma^* N \to M + N$,

GPD extraction from exclusive experiments

Consider a process on a nucleon N, in which a hard scale $|Q^2| \gg \Lambda_{QCD}$ is present.
Factorize the amplitude into perturbatively computable hard part and process-independent Generalised Parton Distributions.

- Deeply Virtual Compton Scattering: $e^- N \to e^- N \gamma$.
  The relevant hard sub-process: $\gamma^* N \to \gamma N$,
- Timelike Compton Scattering: $\gamma N \to \gamma^* N$,
- Deeply Virtual Meson Production: $\gamma^* N \to M + N$,

The considered process:

- Photoproduction of photon pairs with large invariant mass:

$$\gamma N \to \gamma \gamma N$$

Why study this process?

Why study this process?

- The hard part is a $2 \to 3$ reaction – new type of processes studied within the framework of QCD collinear factorization.

Why study this process?

- The hard part is a $2 \to 3$ reaction – new type of processes studied within the framework of QCD collinear factorization.
- The amplitude depends only on charge-odd combinations of GPDs (only valence quarks contribute).

Why study this process?

- The hard part is a $2 \to 3$ reaction – new type of processes studied within the framework of QCD collinear factorization.
- The amplitude depends only on charge-odd combinations of GPDs (only valence quarks contribute).
- No contribution from the badly known chiral-odd quark GPDs at the leading twist.

Kinematics

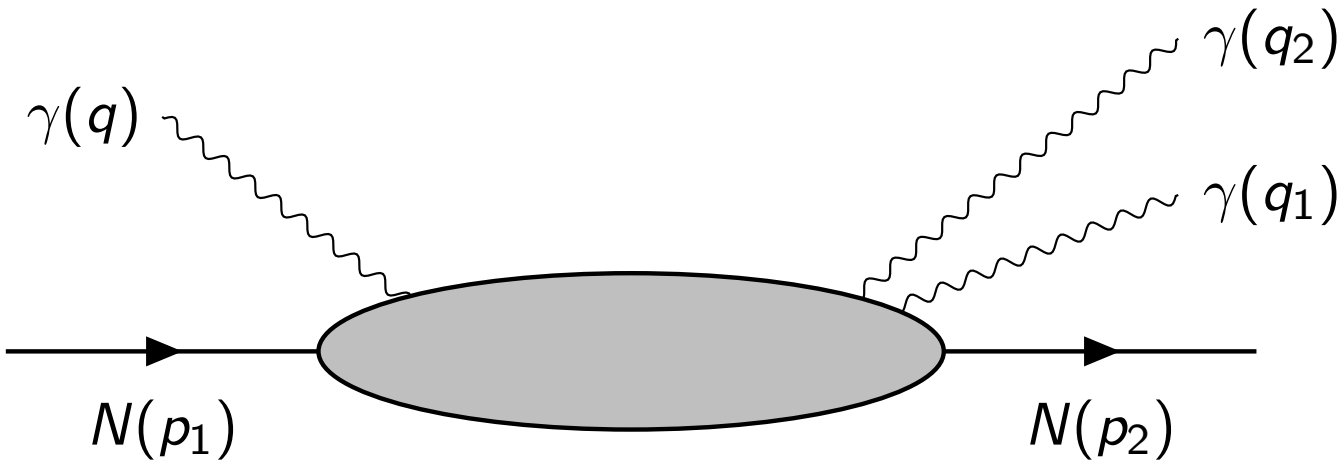

$$S_{\gamma N} = (p_1 + q)^2, \qquad u' = (q_2 - q)^2,$$

$$M^2_{\gamma\gamma} = (q_1 + q2)^2, \qquad t = (p_1 - p_2)^2.$$

Kinematics

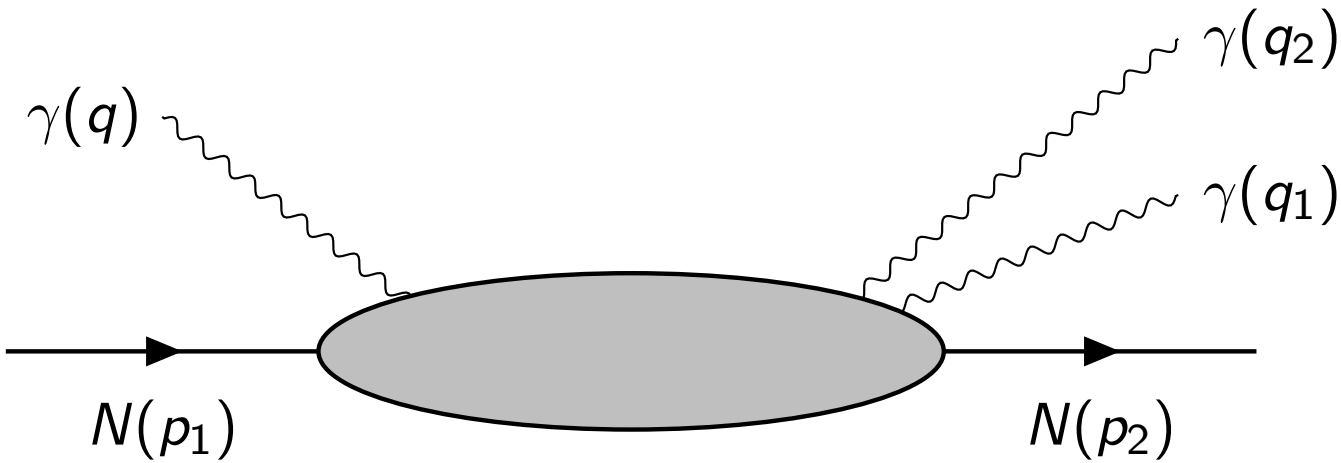

$$S_{\gamma N} = (p_1 + q)^2, \qquad u' = (q_2 - q)^2,$$

$$M^2_{\gamma\gamma} = (q_1 + q2)^2, \qquad t = (p_1 - p_2)^2.$$

$$\xi \approx \frac{M^2_{\gamma\gamma}}{2S_{\gamma N}}.$$

Factorization

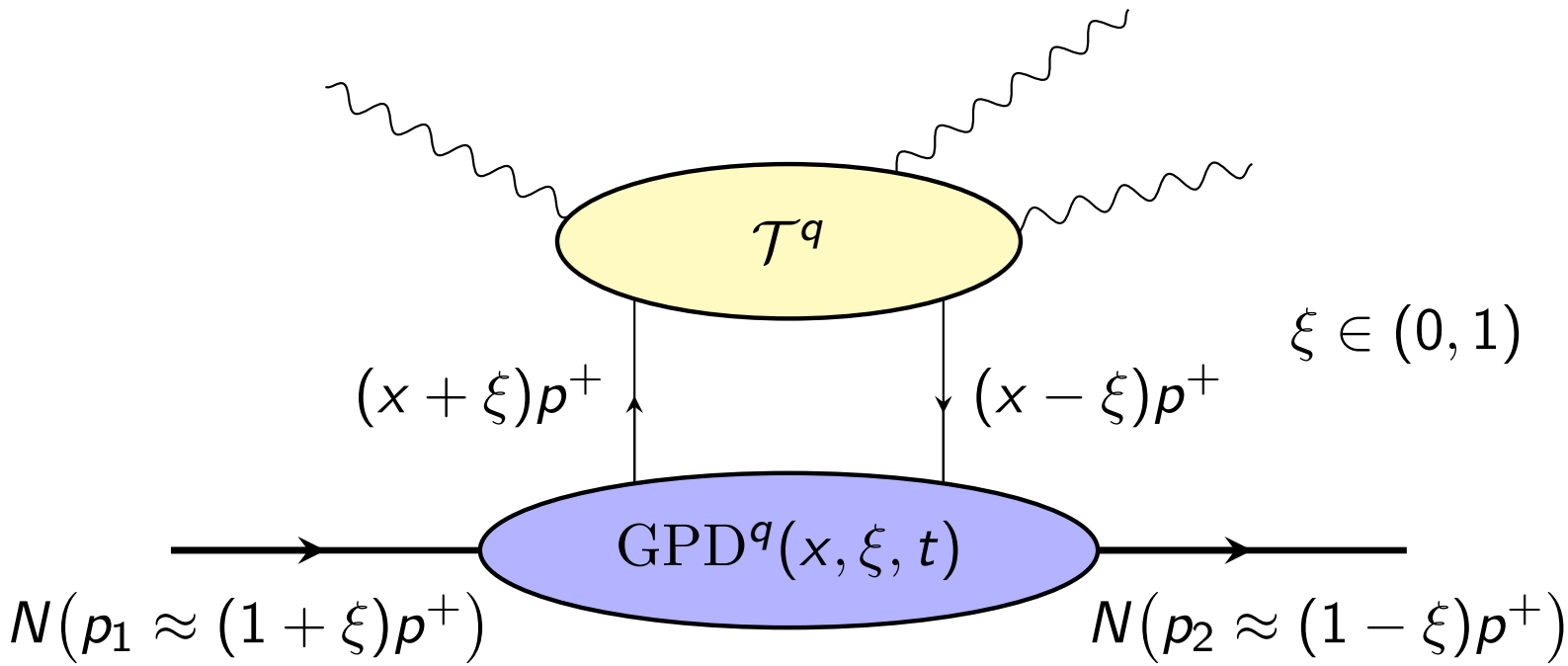

The full amplitude:

$$\mathcal{T} = \sum_q \int_{-1}^{1} dx\, \mathcal{T}^q\big(x,\xi,\ldots\big)\mathrm{GPD}^q(x,\xi,t).$$

The leading order analysis

Pedrak et al. Phys. Rev. D 96 (2017) [arXiv:1708.01043]

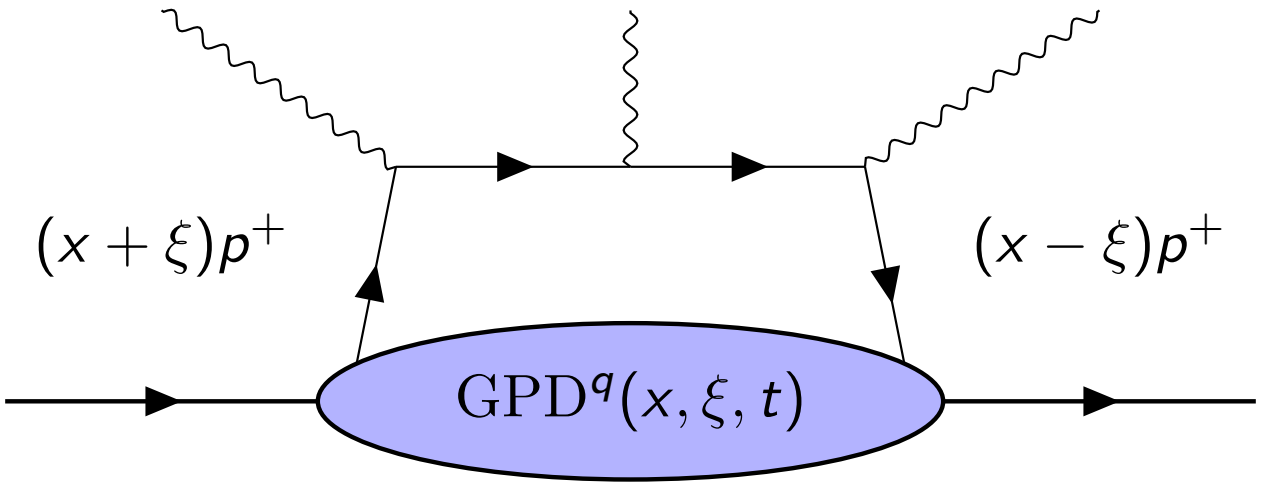

LO results: the process can be studied at intense quasi-real photon beam facilities in JLab or EIC.

Next-to-leading order results

NLO factorization and the amplitude

Phys. Rev. D 104 (2021) [2110.00048]

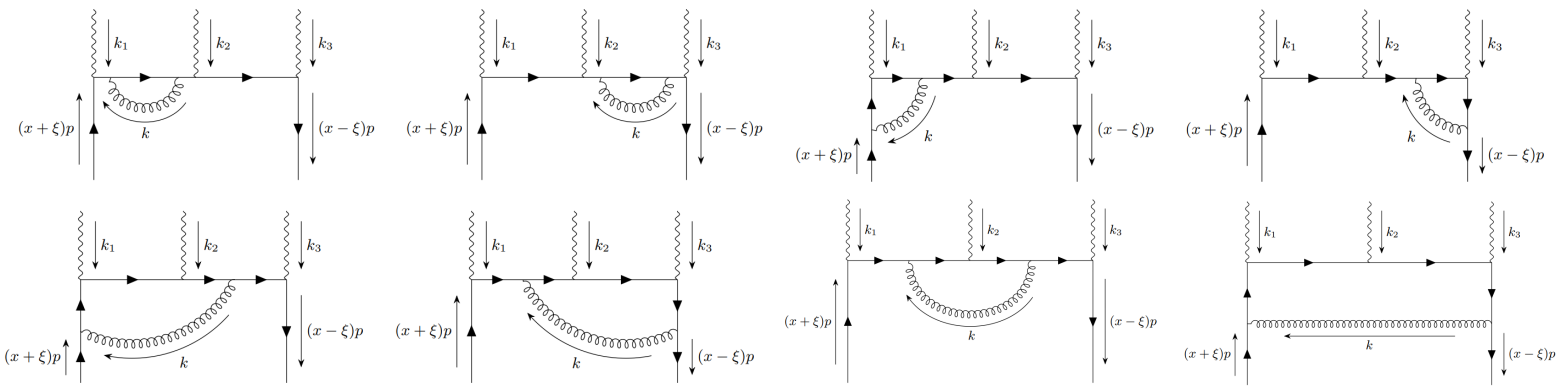

Figure: Considered 1-loop diagrams

Next-to-leading order results

- 2- and 3-point loops $\rightarrow$ relatively simple results.

Next-to-leading order results

- 2- and 3-point loops $\rightarrow$ relatively simple results.
- 5-point loop integral can be reduced to a sum 4-point ones.

Next-to-leading order results

- 2- and 3-point loops $\rightarrow$ relatively simple results.
- 5-point loop integral can be reduced to a sum 4-point ones.
- Finite part of a 4-point diagrams: expressible in terms of

$$\mathcal{F}_{nab} := \int_0^1 dy \int_0^1 dz\, y^a z^b \Big(\alpha_1 y + \alpha_2 z + \alpha_3 yz + i\epsilon\Big)^{-n},$$

$$\mathcal{G} := \int_0^1 dy \int_0^1 dz\, z^2 \Big(\alpha_1 y + \alpha_2 z + \alpha_3 yz + i\epsilon\Big)^{-2} \times \log\Big(\alpha_1 y + \alpha_2 z + \alpha_3 yz + i\epsilon\Big).$$

Next-to-leading order results

- 2- and 3-point loops $\rightarrow$ relatively simple results.
- 5-point loop integral can be reduced to a sum 4-point ones.
- Finite part of a 4-point diagrams: expressible in terms of

$$\mathcal{F}_{nab} := \int_0^1 dy \int_0^1 dz\, y^a z^b \Big(\alpha_1 y + \alpha_2 z + \alpha_3 yz + i\epsilon\Big)^{-n},$$

$$\mathcal{G} := \int_0^1 dy \int_0^1 dz\, z^2 \Big(\alpha_1 y + \alpha_2 z + \alpha_3 yz + i\epsilon\Big)^{-2} \times \log\Big(\alpha_1 y + \alpha_2 z + \alpha_3 yz + i\epsilon\Big).$$

Large computational power is needed to get stable results.

PARTONS

PARtonic Tomography Of Nucleon Software
B. Berthou et al., Eur. Phys. J. C 78, 478 (2018), hep-ph/1512.06174

http://partons.cea.fr

Considered GPD models

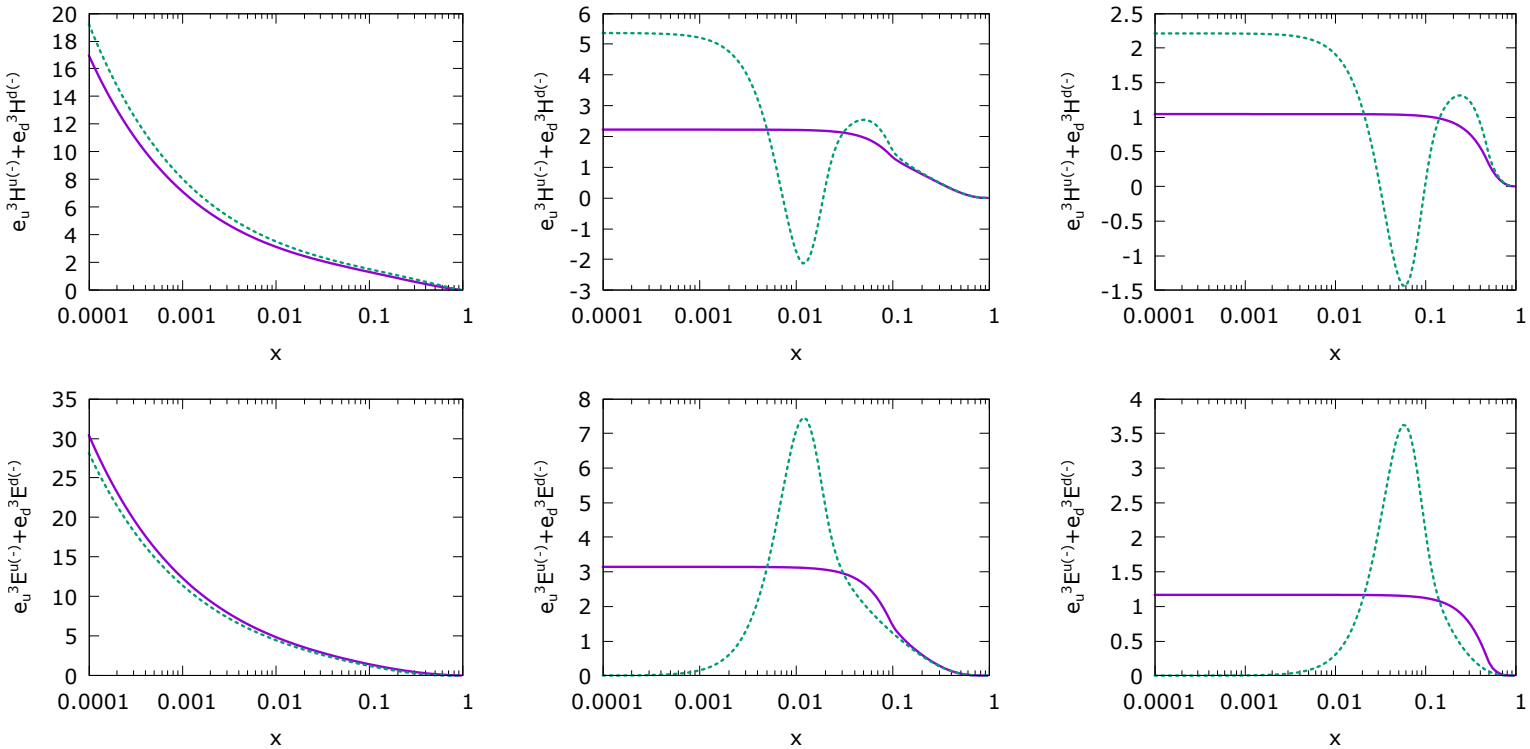

Figure: Comparison between GK [hep-ph/0708.3569] (solid magenta) and MMS [hep-ph/1304.7645] (dotted green) GPD models for $t = -0.1\ \mathrm{GeV}^2$ and the scale $\mu_F^2 = 4\ \mathrm{GeV}^2$.

H^q, E^q - vector GPDs, $\tilde{H}^q, \tilde{E}^q$ - axial GPDs.

H^q, E^q - vector GPDs, $\tilde{H}^q, \tilde{E}^q$ - axial GPDs.

$$\mathcal{H} = \sum_q \int_{-1}^{1} dx\, \mathcal{T}^q(x, \xi, ...) H^q(x, \xi, t),$$

$\mathcal{E}, \tilde{\mathcal{H}}, \tilde{\mathcal{E}}$ defined in the analogous way.

H^q, E^q - vector GPDs, $\tilde{H}^q, \tilde{E}^q$ - axial GPDs.

$$\mathcal{H} = \sum_q \int_{-1}^{1} dx\, \mathcal{T}^q(x, \xi, ...) H^q(x, \xi, t),$$

$\mathcal{E}, \tilde{\mathcal{H}}, \tilde{\mathcal{E}}$ defined in the analogous way.

Contribution from axial GPDs is small at LO, we neglect it in the NLO analysis.

Stability of results

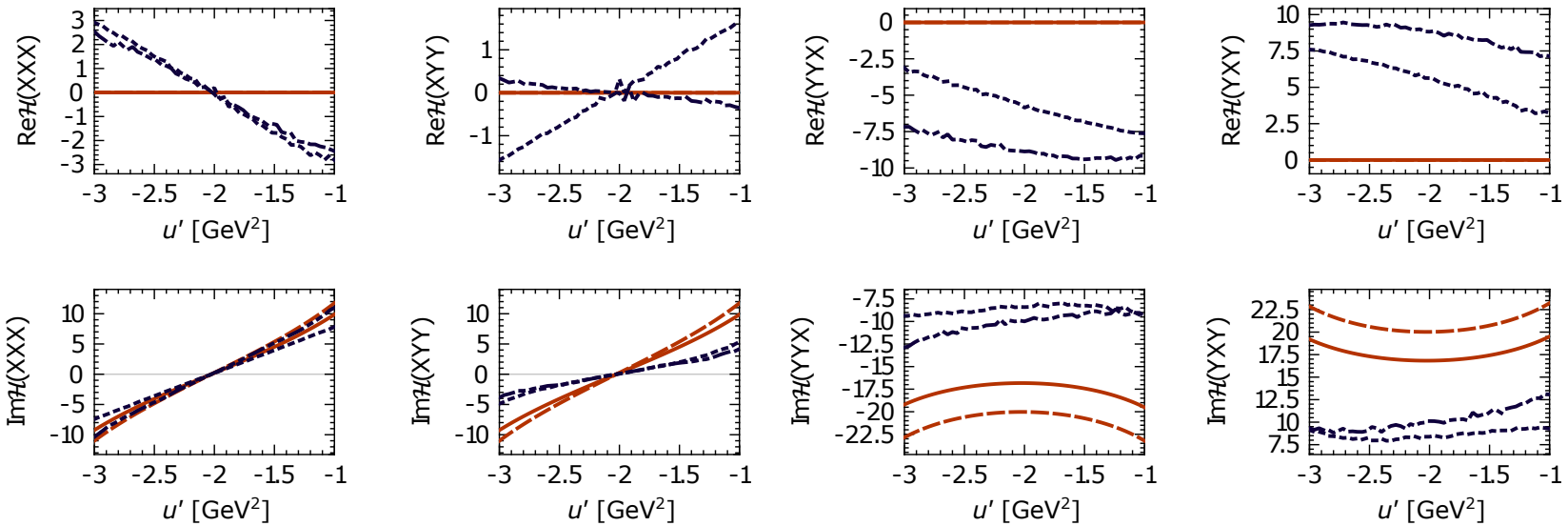

Figure: $\mathcal{H}$ as a function of u' for $S_{\gamma N} = 20\ \mathrm{GeV}^2$, $M^2_{\gamma\gamma} = 4\ \mathrm{GeV}^2$ (which corresponds to $\xi \approx 0.12$) and $t = t_0 \approx -0.05\ \mathrm{GeV}^2$.

Stability of results

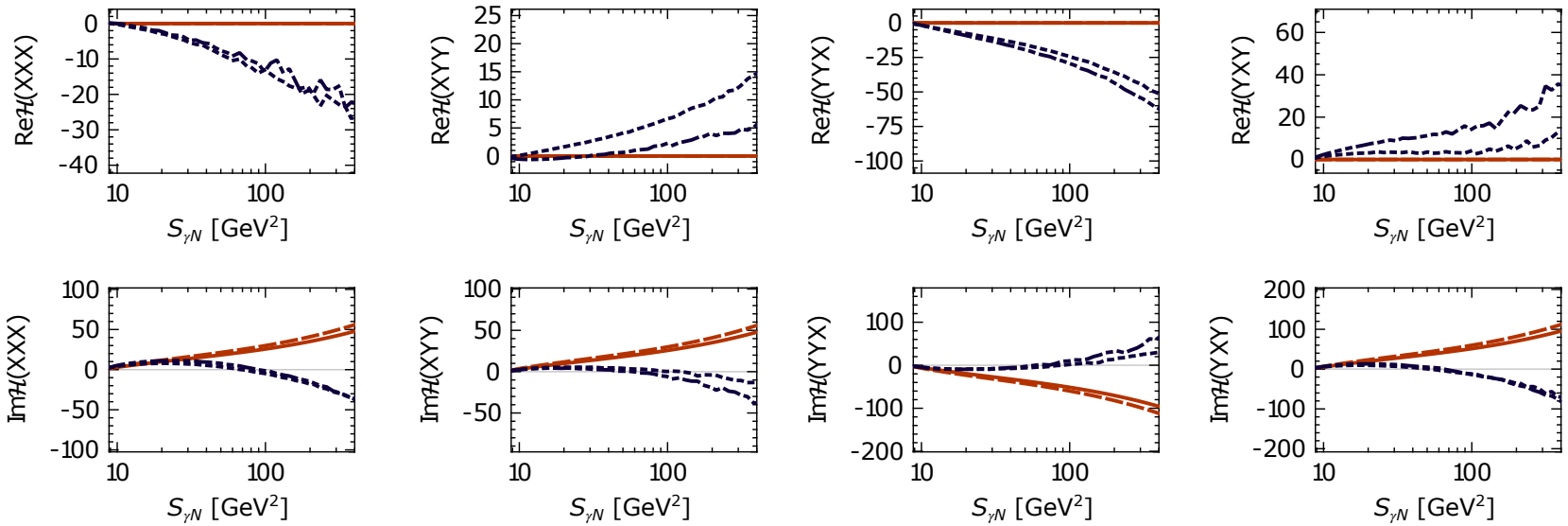

Figure: $\mathcal{H}$ as a function of $S_{\gamma N}$ for $M^2_{\gamma\gamma} = 4\ \mathrm{GeV}^2$, $t = t_0$ and $u' = -1\ \mathrm{GeV}^2$.

Stability of results

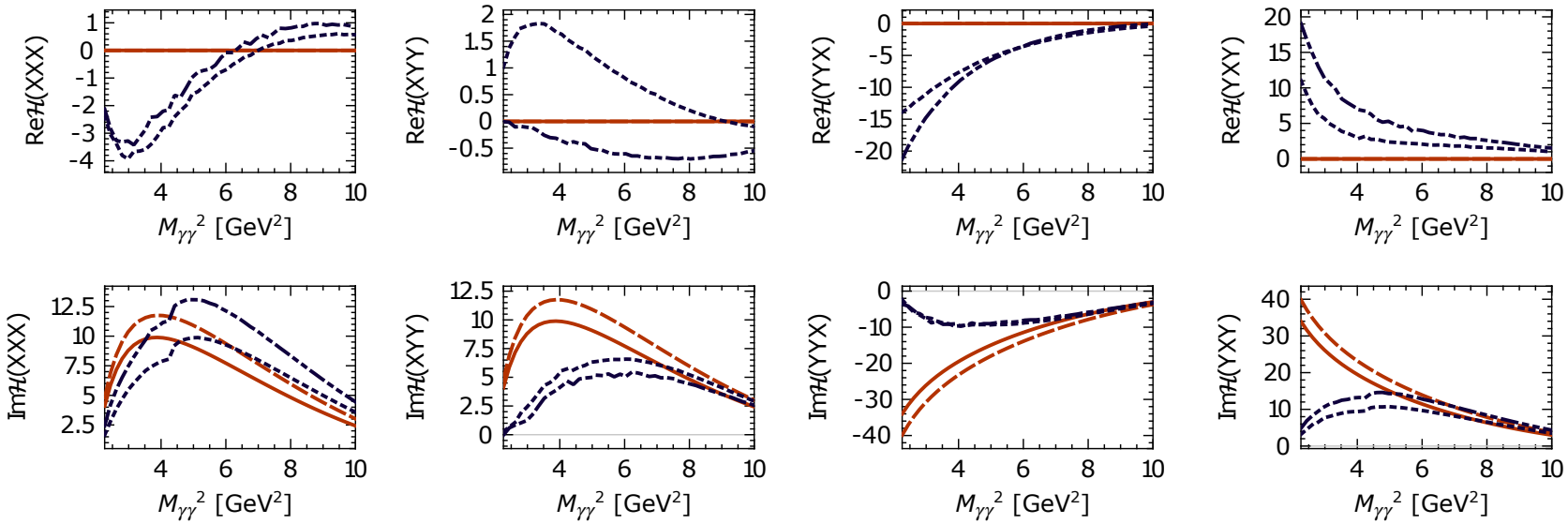

Figure: $\mathcal{H}$ as a function of $M_{\gamma\gamma}$ for $S_{\gamma N} = 20\ \mathrm{GeV}^2$, $t = t_0$ and $u' = -1\ \mathrm{GeV}^2$.

Differential cross section: u'-dependence

$$\frac{d\sigma}{dt\ du'\ dM^2_{\gamma\gamma}}$$

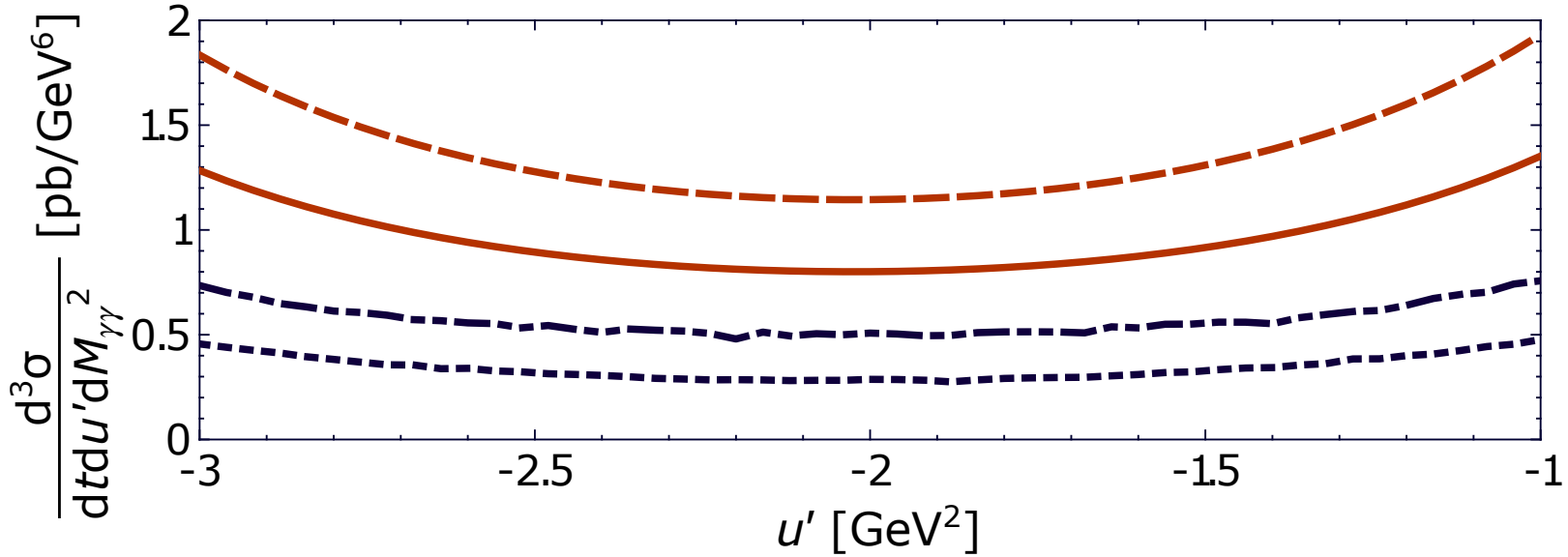

Figure: Differential cross-section as a function of u' for $S_{\gamma N} = 20\ \mathrm{GeV}^2$, $M^2_{\gamma\gamma} = 4\ \mathrm{GeV}^2$ ($\xi \approx 0.12$) and $t = t_0 \approx -0.05\ \mathrm{GeV}^2$ for proton target. LO: solid (dashed) red line, NLO: dotted (dash-dotted) blue line for GK (MMS) GPD model.

Differential cross section: $S_{\gamma N}$-dependence

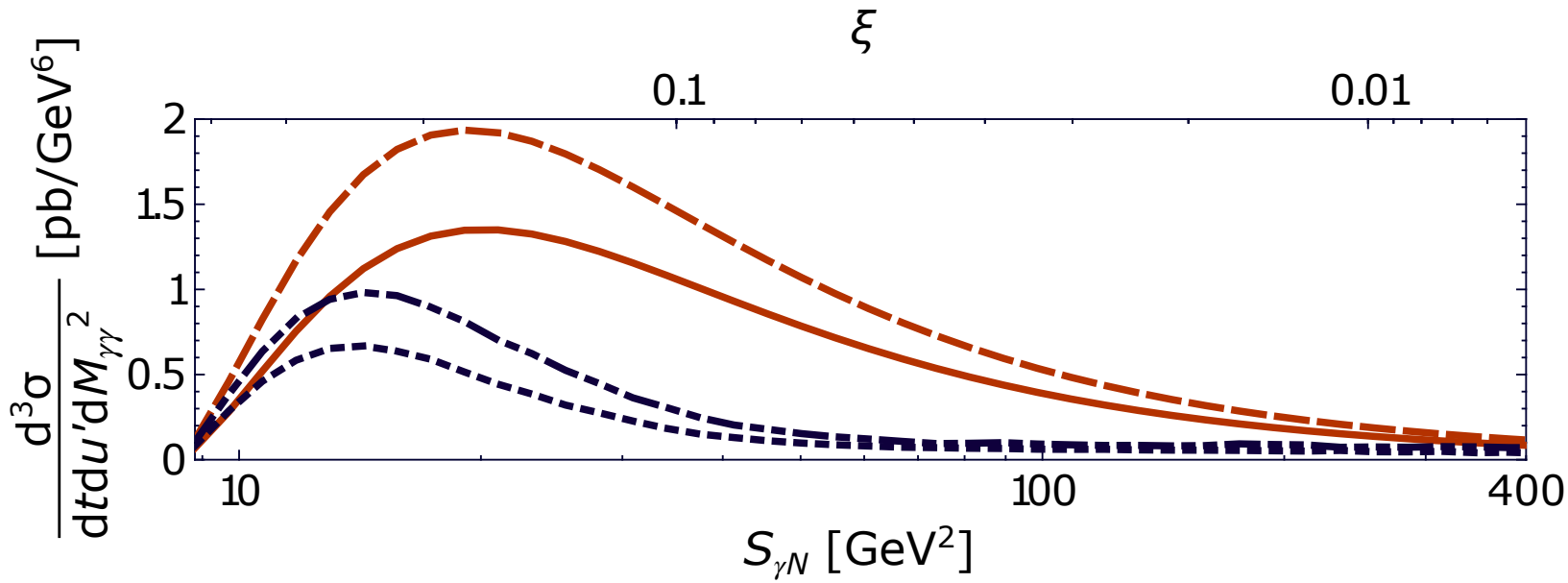

Figure: Differential cross-section as a function of $S_{\gamma N}$ (bottom axis) and the corresponding ξ (top axis) for $M^2_{\gamma\gamma} = 4\ \mathrm{GeV}^2$, $t = t_0$ and $u' = -1\ \mathrm{GeV}^2$.

Differential cross section: $S_{\gamma N}$-dependence

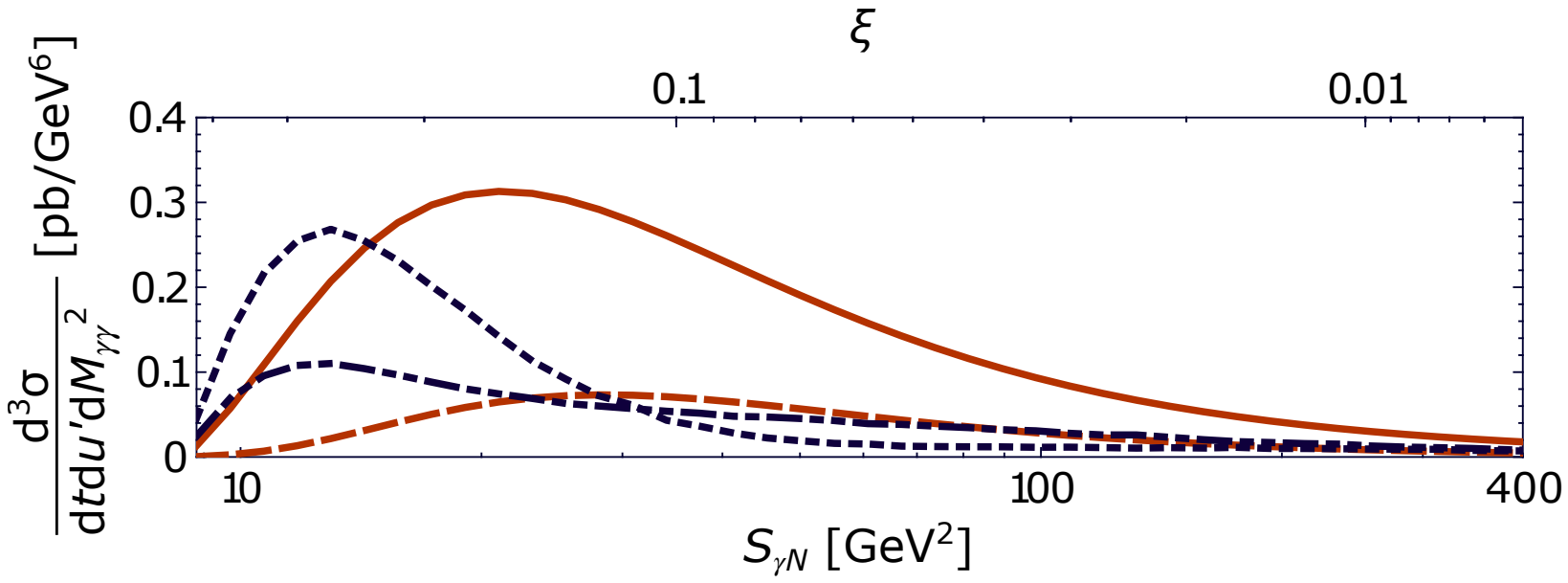

Figure: The same, but for neutron target.

Differential cross section: $M^2_{\gamma\gamma}$-dependence

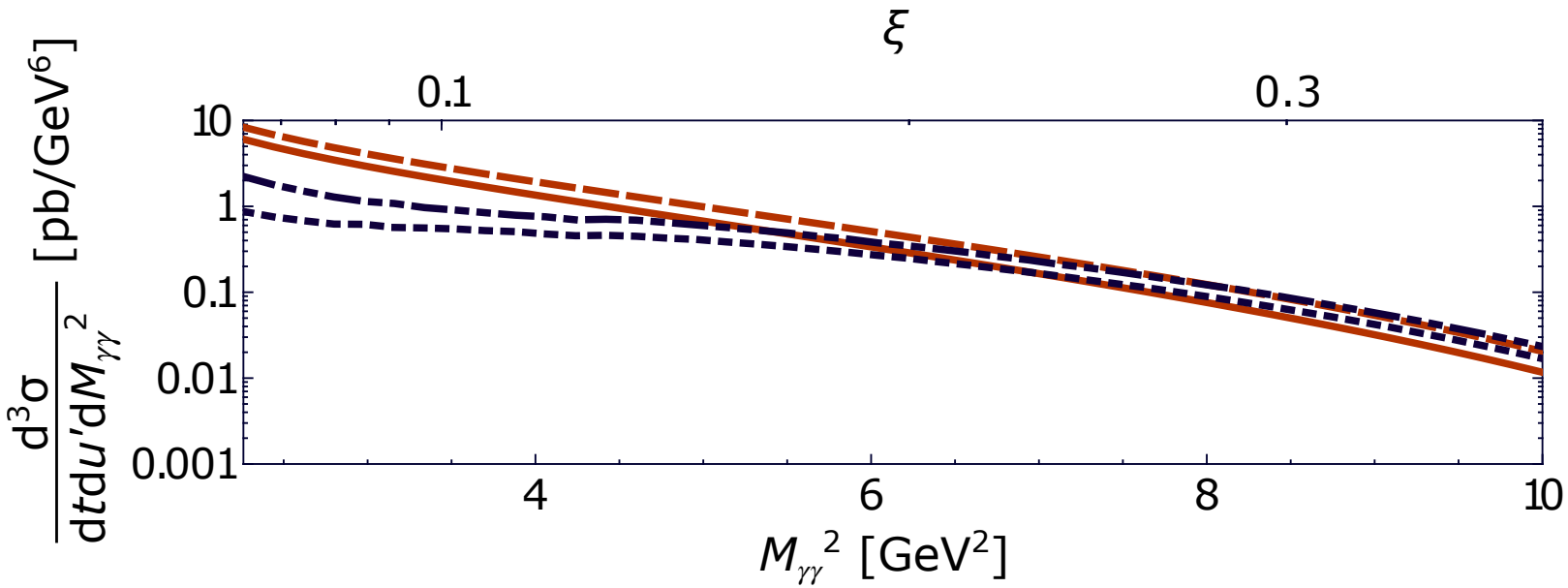

Figure: Differential cross-section as a function of $M^2_{\gamma\gamma}$ (bottom axis) and the corresponding ξ (top axis) for $S_{\gamma N} = 20\ \mathrm{GeV}^2$, $t = t_0$ and $u' = -1\ \mathrm{GeV}^2$.

Differential cross section: ϕ-dependence

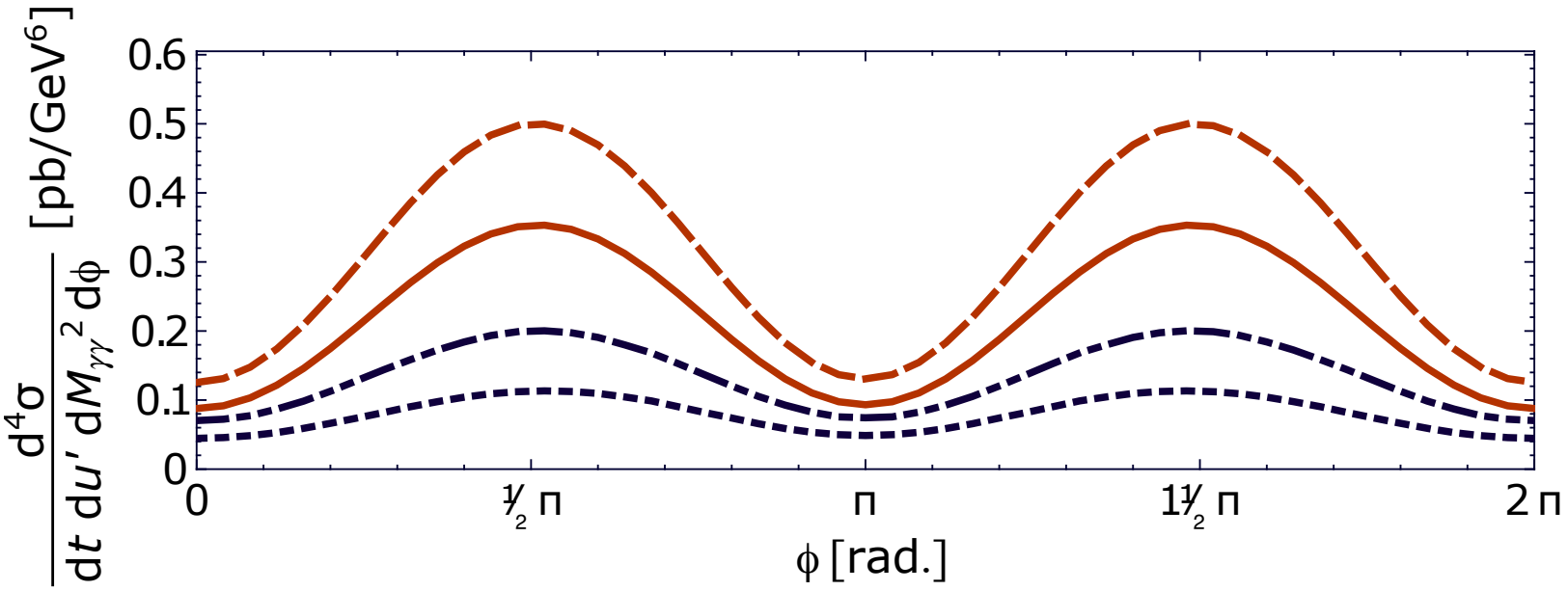

Figure: Differential cross-section as a function of ϕ – the angle between the initial photon polarization and one of the final photon momentum in the transverse plane for $S_{\gamma N} = 20\ \mathrm{GeV}^2$, $M_{\gamma\gamma}^2 = 4\ \mathrm{GeV}^2$ (which corresponds to $\xi \approx 0.12$), $u' = -1\ \mathrm{GeV}^2$ and $t = t_0 \approx -0.05\ \mathrm{GeV}^2$.

Summary

Summary

- $\gamma N \to \gamma\gamma N$ can provide valuable information about charge-odd combinations of GPDs,

Summary

- $\gamma N \to \gamma\gamma N$ can provide valuable information about charge-odd combinations of GPDs,
- We performed a next-to-leading order analysis of the diphoton photoproduction process,

Summary

- $\gamma N \to \gamma\gamma N$ can provide valuable information about charge-odd combinations of GPDs,
- We performed a next-to-leading order analysis of the diphoton photoproduction process,
- NLO corrections result in smaller cross sections,

Summary

- $\gamma N \to \gamma\gamma N$ can provide valuable information about charge-odd combinations of GPDs,
- We performed a next-to-leading order analysis of the diphoton photoproduction process,
- NLO corrections result in smaller cross sections,
- Due to complicated form of the NLO amplitude, a large computational power is needed to reduce the numerical noise.

Backup: Transverse target asymmetry

ϕ_{Δ_T,S_T} – relative angle between transverse momentum of outgoing nucleon and the initial polarization vector.
The moment of this asymmetry:

$$\mathcal{A}^{\sin(\phi_{\Delta_T,S_T})} = \frac{1}{\pi}\int_0^{2\pi} \mathrm{d}(\phi_{\Delta_T,S_T})\mathcal{A}\sin(\phi_{\Delta_T,S_T})\,, \qquad (1)$$

LO: the asymmetry is exactly 0, while at NLO it is small, but non-vanishing.

Backup: Transverse target asymmetry

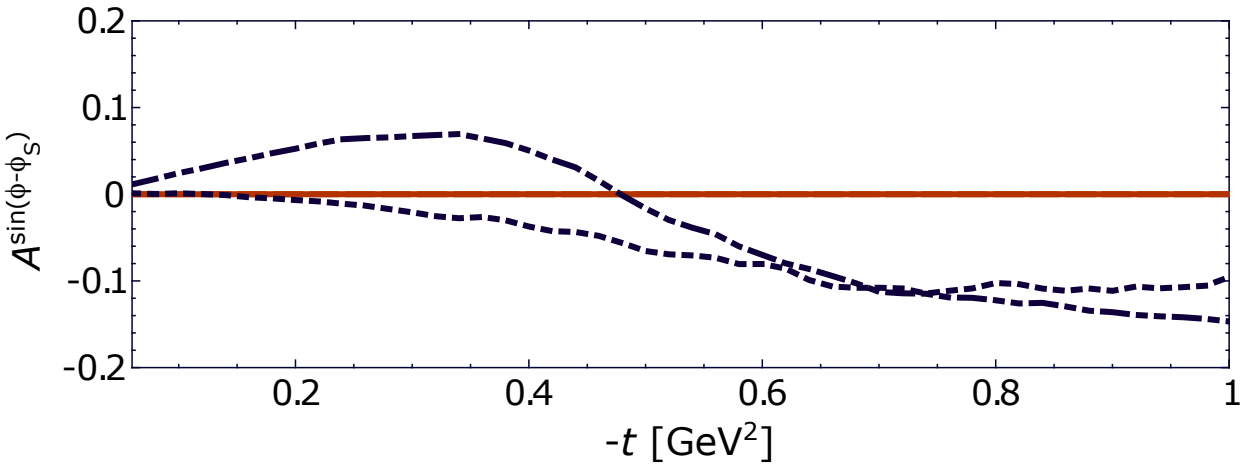

Figure: The transverse target asymmetry $\mathcal{A}^{\sin(\phi_{\Delta T}, s_T)}$ as a function of $-t$ for $S_{\gamma N} = 20\ \mathrm{GeV}^2$, $M^2_{\gamma\gamma} = 4\ \mathrm{GeV}^2$ (which corresponds to $\xi \approx 0.12$) and $u' = -1\ \mathrm{GeV}^2$.